

Encapsulation of Flavin Cofactor within a Manganese Porphyrin-Based Metal–Organic Polyhedron for Reductive Dioxygen Activation

LiLi Li, Huimin Guo, Linlin Yang, Xuezhao Li, Hailing Wang, and Cheng He*



Cite This: <https://dx.doi.org/10.1021/acs.inorgchem.9b03430>



Read Online

ACCESS |



Metrics & More



Article Recommendations



Supporting Information

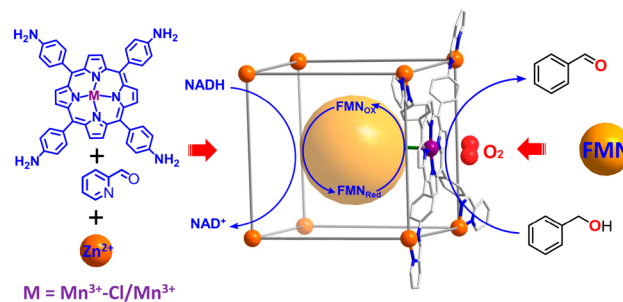
ABSTRACT: Encapsulation of flavin mononucleotide (FMN) in a porphyrinatomanganese(III)-based cubic cage allowed the fast reduction of manganese(III) porphyrin in the presence of nicotinamide adenine dinucleotide (NADH). This supramolecular system was capable of efficiently activating dioxygen and catalyzing the oxidation of benzyl alcohol. Control experiments suggested that the close proximity between FMN and manganese(III) porphyrins forced by the host–guest interaction might benefit the electron-transfer process from the FMN cofactor to the metal centers.

To design and prepare supramolecular systems that echo the remarkable reactivity of natural enzymes, chemists have constructed “molecular containers” with defined cavities to catalyze unique chemical transformations with high efficiency and selectivity based on their local microenvironments.¹ Among these containers, coordination-driven-assembled metal–organic polyhedra are good candidates for emulating the properties of enzyme active sites.² These well-designed hosts can provide unique confined environments for encapsulated complementary guest molecules³ and have the potential to achieve the selectivity and catalytic rate enhancements displayed by biological systems.⁴ Additionally, the components being forced closer within the inner space, leading to an efficient enhancement in energy, electron, or substance transfer, has also attracted much attention.⁵

In living organisms, cytochromes P450 (CYPs) composed of cytochrome P450 reductase (CPR) and cytochrome P450 are multidomain enzymes that play important roles in the oxidation of various xenobiotics and metabolites through the reductive activation of dioxygen.^{6,7} CPR consists of flavin adenine dinucleotide/flavin mononucleotide (FMN) cofactors, which collect electron pairs as hydride ions from NAD(P)H and, in turn, transfer electrons to the metal centers of cytochrome P450 (heme). The reduced metal center of heme then activates a dioxygen molecule, which accepts an electron from CPR.⁸ In each electron-transfer (ET) step, interactions between different domains are the key factor affecting rapid and controlled ET in multicomponent systems.^{9–11} Interactions between the reduced pyridine–dinucleotide cofactors and flavins have been investigated by adjusting their mutual relative positions through covalent and noncovalent binding.^{12–14} However, crucial cytochrome P450 research into the ET process between flavins and heme metal centers, which is more complex owing to the heme metal centers being vulnerable to the impact of substrates and other electron donors,^{7c,10} still remains challenging.

Inspired by the significant advances in efficient host–guest ET within cage-like hosts,¹⁵ we envisaged that such a supramolecular strategy might also provide an approach to mimicking cytochrome P450 enzymes. As metalloporphyrins are widely applied as synthetic models for cytochrome P450 enzymes,¹⁶ herein, we constructed an artificial reductase system with FMN encapsulated in a self-assembled cubic M_8L_6 cage¹⁷ consisting of Mn(III)-porphyrin moieties (Scheme 1). In the cavity of the cubic Mn(III)-porphyrin

Scheme 1. Schematic of Artificial Reductase System Showing FMN Encapsulation and Benzyl Alcohol Oxidation



cage, FMN is expected to collect electron pairs from nicotinamide adenine dinucleotide (NADH), with reduced FMN able to efficiently reduce Mn(III)-porphyrin to the corresponding Mn(II)-porphyrin in a stepwise single-electron process. Furthermore, the formed Mn(II)-porphyrin intermediate activates dioxygen to realize an aromatic alcohol oxidation catalysis process.

Received: November 22, 2019

Treating 2-formylpyridine (24 equiv) with tetrakis(4-aminophenyl)porphyrinatomanganese(III) (Mn-TAPP; 6 equiv) in the presence of Zn(NTf₂)₂ (8 equiv) and ¹⁸Bu₄NPF₆ (6 equiv) resulted in the formation of complex Zn₈(L-Cl)₆(NTf₂)₁₆ [**cubic-(Mn^{III}Cl)**; L = manganese(III) 5,10,15,20-tetrayltetrakis(benzene-4,1-diyl)tetrakis[1-(pyridin-2-yl)methanimine]porphine; Scheme S2]. Slow diffusion of diethyl ether into the solution of **cubic-(Mn^{III}Cl)** afforded crystals suitable for X-ray diffraction analysis. As shown in Figure 1, **cubic-(Mn^{III}Cl)** crystallized in the monoclinic space

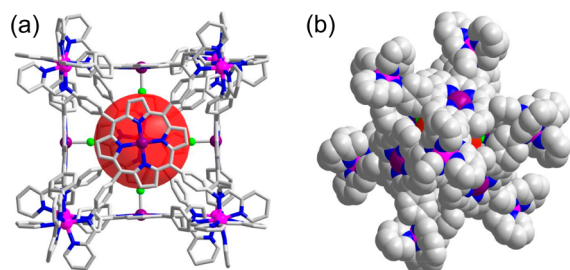


Figure 1. Crystal structure of **cubic-(Mn^{III}Cl)** showing the coordination geometries of Zn(II) and Mn(II) ions and empty spheres (red balls) for guest encapsulation. Solvent molecules, anions, and H atoms were omitted for clarity.

group *C2/c*, with half of the cubic cage in an asymmetric unit. This arrangement of metal ions and coordination ligands led to a cubic cage, with the eight vertices occupied by Zn ions and the six faces occupied by the manganese porphyrin-based ligand. Meanwhile, the Cl⁻ ion served as the axial ligation to each manganese porphyrin and was coordinated to manganese inside/outside (disordered in a 2:1 ratio) of the cage at a Mn^{III}–Cl distance of 2.38 Å. The average Mn–Mn distance between opposite faces was approximately 14.5 Å, and the inner void volume was about 1436 Å³.¹⁸ However, because of the paramagnetic nature of Mn(III), the fine NMR spectra could not be obtained.

The electrospray ionization mass spectrometry (ESI-MS) spectrum of **cubic-(Mn^{III}Cl)** in CH₃CN exhibited signals at *m/z* 891.88, 1022.29, 1185.19, and 1394.49 (Figure S2). A simple comparison with the simulation results based on the natural isotopic abundances suggested that the peaks corresponded to [Zn₈L₆Cl₆(NTf₂)_{*n*}]^{(16-*n*)+} (*n* = 6–9). FMN is a biomolecule produced from riboflavin (vitamin B₂) by the enzyme riboflavin kinase and functions as the prosthetic group of CPR, with phosphorylated anion groups at its terminal. The positively charged **cubic-(Mn^{III}Cl)** most likely allowed FMN encapsulation in its cavity. The ESI-MS spectrum of **cubic-(Mn^{III}Cl)** in the presence of excess FMN exhibited new intense peaks at *m/z* 1253.30, 1472.32, and 1764.46, which were clearly assigned to [Zn₈L₆Cl₅(FMN)(NTf₂)_{*n*}(CH₃CN)₃]^{(16-*n*)+} (*n* = 8–10), indicating the binding of one FMN molecule in the host (Figure S3), and one of the chloride ions was dissolved from the Mn(III) center. The density functional theory (DFT) results also suggested that FMN could be encapsulated inside the Mn^{III}Cl cage. The strong affinity of Mn(III) to the negatively charged phosphate moiety accounts for the encapsulation (Figure S17).

An isothermal titration calorimetry (ITC) experiment was conducted to better understand the guest binding interactions between **cubic-(Mn^{III}Cl)** and FMN. The observed inclusion number was 1.0, as determined by an independent model

(Figure S14). The association constant calculated from the ITC titration was 1.6 × 10⁵ M⁻¹. Furthermore, fluorescence titration experiments were performed to study the guest FMN binding ability of the **cubic-(Mn^{III}Cl)** cage. Adding **cubic-(Mn^{III}Cl)** (6.25 μM) to a CH₃CN/H₂O solution of FMN (10 μM) quenched approximately 70% of the emission intensity of FMN (Figure 2), suggesting that FMN interacted strongly with

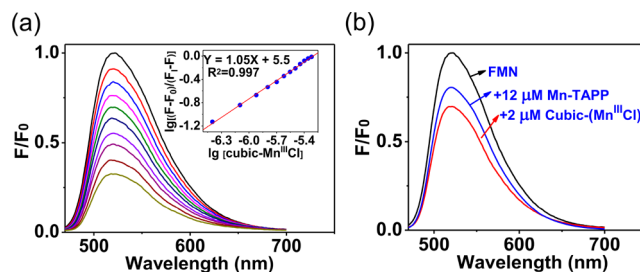


Figure 2. (a) Emission spectra of FMN (10 μM) (black line) upon the addition of **cubic-(Mn^{III}Cl)** up to 6.25 μM. Inset: Hill plot of the titration curve of fluorescein upon the addition of **cubic-(Mn^{III}Cl)** showing the associate constant. (b) Luminescence spectra of FMN (10 μM, black line) in CH₃CN/H₂O (1:1) upon the addition of **cubic-(Mn^{III}Cl)** (2.0 μM, red line) and Mn-TAPP (12 μM, blue line).

cubic-(Mn^{III}Cl). A Hill plot with the fitting curve of the profile indicated the formation of a 1:1 complex with an association constant of 3.1 × 10⁵ M⁻¹. Both the large association constant and 1:1 stoichiometric ratio suggested the formation of a stable FMN@**cubic-(Mn^{III}Cl)** host–guest complex in solution. In contrast, the association constant of NADH with **cubic-(Mn^{III}Cl)** (Figure S15) was 2.6 × 10⁴ M⁻¹, which was much lower than that of FMN, indicating that FMN bound more strongly with **cubic-(Mn^{III}Cl)** compared with the larger-sized NADH at the same concentration, while luminescence titrations of FMN (10 μM) with the addition of Mn-TAPP (12 μM) quenched about 20% and gave a quenching constant (*K_{sv}*) of about 5.7 × 10⁴ M⁻¹. Meanwhile, adding **cubic-(Mn^{III}Cl)** (2 μM) to FMN (10 μM) quenched approximately 30% of the intensity (Figure 2b). Obviously, the quenching efficiency of **cubic-(Mn^{III}Cl)** was higher than that of Mn-TAPP.

The catalytic activities of most CYPs require one or more redox partner proteins to sequentially deliver two electrons from NADH to the heme metal reactive center for dioxygen activation.¹⁹ The possible ET between NADH and the FMN@**cubic-(Mn^{III}Cl)** supermolecular system was investigated. Changes in the UV–vis spectra of FMN@**cubic-(Mn^{III}Cl)** were recorded to study its reduction by NADH. Manganese(III) and -(II) porphyrins have distinctive absorption bands at 470 and 440 nm, respectively.^{13,20} Upon the addition of NADH to FMN@**cubic-(Mn^{III}Cl)** in *N,N*-dimethylformamide (DMF)/acetonitrile (CH₃CN) (1:1), the absorption band at 470 nm gradually decreased and a new band at 440 nm was observed (Figure S7a), reaching equilibrium within 30 min. The appearance of clear isosbestic points at 418, 458, and 584 nm also demonstrated the direct one-electron reduction of manganese(III) porphyrin, with no other intermediate observed. Finally, once exposed to dioxygen, this Mn(II) was rapidly reoxidized to Mn(III) with the same isosbestic points (Figure S7b).

The reduction potential measured by the cyclic voltammetry experiments for **cubic-(Mn^{III}Cl)** in DMF/CH₃CN (1:1,

v/v) was -728 mV (vs Fc^+/Fc ; Figure S5). On the basis of previous equilibrium measurements for enzyme-catalyzed reactions, the thermodynamic redox potential for the NAD^+/NADH couple was estimated to be -997 mV (vs Fc^+/Fc),²¹ which is low enough to reduce manganese(III) porphyrin.

The reduction experiment was performed in the absence of FMN with NADH ($30 \mu\text{M}$) added to **cubic-(Mn^{III}Cl)** ($5 \mu\text{M}$) in DMF/ CH_3CN (1:1, v/v) under argon. The Mn(II) absorbances at around 440 and 470 nm increased and decreased, respectively, indicating the reduction of Mn(III) (Figure S9). The initial reaction rate calculated from the fitting curve was $2 \times 10^{-8} \text{ M min}^{-1}$, as shown in Figure 3b (control

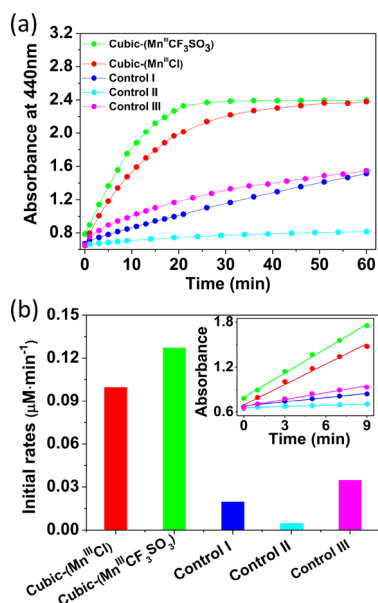


Figure 3. (a) Time dependence of Mn(III) reduction under argon conditions by recording reduced Mn(II) at 440 nm, in the presence of **cubic-(Mn^{III}Cl)** ($5 \mu\text{M}$), NADH ($30 \mu\text{M}$), and FMN ($5 \mu\text{M}$, red circle). (b) Comparison of the initial reduction reaction rates of manganese(III) porphyrin under different conditions. Inset: Plot fitting of the kinetic initial reaction rates of the manganese(III) porphyrin process under different conditions.

I), which was around one-fifth of that in the presence of FMN. This result demonstrated that the FMN cofactor was essential to facilitate ET in the reduction process, as found in nature.^{7,8}

Control experiments with Mn-TAPP instead of **cubic-(Mn^{III}Cl)** were also conducted for comparison (control II). The time-dependent reduction experiment of monomeric Mn-TAPP [$30 \mu\text{M}$, maintaining the same Mn(III) concentration as that in **cubic-(Mn^{III}Cl)**] was performed. However, the reduction process was much slower than that with **cubic-(Mn^{III}Cl)** (Figure S8). The initial reaction rates were measured as $1.0 \times 10^{-7} \text{ M min}^{-1}$ for **cubic-(Mn^{III}Cl)** and only $5.0 \times 10^{-9} \text{ M min}^{-1}$ in the case of Mn-TAPP (Figure 3b). The superiority of the host–guest system should be attributed to the close proximity between the FMN and metal redox centers within the host–guest system, which was beneficial to the efficient ET process.^{10,12a}

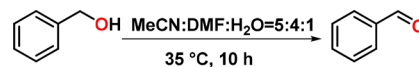
A similar but nonreactive species, adenosine triphosphate [ATP; $K_a = 1.08 \times 10^{-5} \text{ M}^{-1}$ for **cubic-(Mn^{III}Cl)**; Figure S16] was chosen as the inhibitor to illustrate the supramolecular feature of the system. The addition of ATP (0.16 mM) to the solution mixture containing FMN ($10 \mu\text{M}$) and **cubic-**

(**Mn^{III}Cl**) ($10 \mu\text{M}$) resulted in an emission recovery of the same band, while the addition of ATP (0.5 mM) to the solution of FMN ($10 \mu\text{M}$) did not cause any quenching of the emission of FMN (Figure S13), suggesting substitution of the encapsulated FMN in the pocket of **cubic-(Mn^{III}Cl)** by ATP. The inhibition experiment was carried out by adding an excess of ATP to the reaction mixture (control III). As shown in Figure 3, the addition of an excess of ATP ($160 \mu\text{M}$) efficiently reduced the reaction rate to $3.0 \times 10^{-8} \text{ M min}^{-1}$.

Cl^- occupation of the cage cavity can potentially affect the rate of oxidized FMN exchange and obstruct oxygen molecule activation. Anion metathesis with AgCF_3SO_3 was employed to replace coordinated Cl^- located on the porphyrin metal centers with weakly coordinated CF_3SO_3^- . The noncoordinating manganese porphyrin cage $\text{Zn}_8(\text{L})_6(\text{OTf})_{22}$, abbreviated as **cubic-(Mn^{III}CF₃SO₃)**, was obtained.²² The experiment was conducted using **cubic-(Mn^{III}CF₃SO₃)** instead of **cubic-(Mn^{III}Cl)**, showing a higher rate of Mn(III) reduction ($1.28 \times 10^{-7} \text{ M min}^{-1}$).

The present cubic cage featuring fast ET might efficiently accelerate C–H oxygenation in the presence of NADH and FMN. Supramolecular catalysis in this novel system proceeded using dioxygen as the oxidant with aromatic alcohols as the target substrates. In a model reaction, the C–H oxygenation experiment of benzyl alcohol was performed in Table 1.

Table 1. Control Experiments of C–H Oxygenation of Benzyl Alcohols



entry	catalyst	addition	yield (%)
1	cubic-(Mn^{III}Cl) (2 mol %)	FMN (2 mol %), NADH (50 mol %)	19
2	cubic-(Mn^{III}Cl) (2 mol %)	FMN (2 mol %)	6
3	cubic-(Mn^{III}Cl) (2 mol %)	NADH (50 mol %)	4
4	cubic-(Mn^{III}CF₃SO₃) (2 mol %)	FMN (2 mol %), NADH (50 mol %)	22
5	Mn-TAPP (12 mol %)	FMN (12 mol %), NADH (50 mol %)	8
6	cubic-(Mn^{III}CF₃SO₃) (2 mol %)		0.4
7		FMN (2 mol %), NADH (50 mol %)	0.5
8	cubic-(Mn^{III}Cl) (2 mol %)	FMN (2 mol %), NADH (50 mol %), ATP (32 mol %)	5.5

In entry 1, the mixture was stirred at room temperature for 10 h under an oxygen atmosphere (O₂ at 1 atm), affording a 19% yield of the aldehyde product. **Cubic-(Mn^{III}CF₃SO₃)** was also used as the oxidation catalyst, affording a yield of 22%. Control experiments with the absence of FMN or NADH, and in the presence of Mn-TAPP instead of **cubic-(Mn^{III}Cl)**, showed lower reaction yields. The superiority of this supramolecular system in promoting the oxidation reaction was also extended to several types of benzyl alcohol with modest yields (18–28%, Table S2).

In summary, a manganese porphyrin-based redox-active cubic cage with large cavity sizes was constructed to encapsulate FMN in the internal cavity. The host–guest

interaction system between the flavin cofactor and metal active sites closely resembled the possible ET progress in CPR. This new supramolecular system efficiently collected electron pairs from NADH and rapidly delivered single electrons to manganese(III) porphyrin, with 20-fold rate enhancement compared with the monomer in solution. Meanwhile, this supramolecular system was able to activate dioxygen at the metal centers and catalyze the oxidation of benzyl alcohols in the presence of NADH, using dioxygen as the oxygen source. Manipulating the electronic properties of building blocks and host–guest encapsulation in coordination cages can control the ET process, which will promote the design of functional molecular containers for supramolecular enzyme simulation.

■ ASSOCIATED CONTENT

SI Supporting Information

The Supporting Information is available free of charge at <https://pubs.acs.org/doi/10.1021/acs.inorgchem.9b03430>.

Measurements and materials, syntheses and characterizations, single-crystal X-ray crystallography, ESI-MS spectra, cyclic voltammograms, UV–vis absorption and fluorescence spectra, ITC, DFT calculations, and typical procedure for the C–H oxygenation of benzyl alcohol and related substrates (PDF)

Accession Codes

CCDC 1893668 contains the supplementary crystallographic data for this paper. These data can be obtained free of charge via www.ccdc.cam.ac.uk/data_request/cif, or by emailing data_request@ccdc.cam.ac.uk, or by contacting The Cambridge Crystallographic Data Centre, 12 Union Road, Cambridge CB2 1EZ, UK; fax: +44 1223 336033.

■ AUTHOR INFORMATION

Corresponding Author

Cheng He – State Key Laboratory of Fine Chemicals, Dalian University of Technology, Dalian 116024, P. R. China; orcid.org/0000-0002-1426-0124; Email: hecheng@dlut.edu.cn

Authors

LiLi Li – State Key Laboratory of Fine Chemicals, Dalian University of Technology, Dalian 116024, P. R. China
Huimin Guo – State Key Laboratory of Fine Chemicals, Dalian University of Technology, Dalian 116024, P. R. China; orcid.org/0000-0001-9283-7374
Linlin Yang – Xinxiang Key Laboratory of Forensic Science Evidence, School of Forensic Medicine, Xinxiang Medical University, Xinxiang 453003, P. R. China
Xuezhao Li – State Key Laboratory of Fine Chemicals, Dalian University of Technology, Dalian 116024, P. R. China
Hailing Wang – State Key Laboratory of Fine Chemicals, Dalian University of Technology, Dalian 116024, P. R. China

Complete contact information is available at: <https://pubs.acs.org/doi/10.1021/acs.inorgchem.9b03430>

Funding

This work was supported by the National Natural Science Foundation of China (Grants U1608224 and 21861132004).

Notes

The authors declare no competing financial interest.

■ REFERENCES

- (1) (a) Cullen, W.; Misuraca, M. C.; Hunter, C. A.; Williams, N. H.; Ward, M. D. Highly efficient catalysis of the Kemp elimination in the cavity of a cubic coordination cage. *Nat. Chem.* **2016**, *8*, 231–236. (b) Kaphan, D. M.; Levin, M. D.; Bergman, R. G.; Raymond, K. N.; Toste, F. D. A supramolecular microenvironment strategy for transition metal catalysis. *Science* **2015**, *350*, 1235–1238. (c) Hooley, R. J. Taking on the turnover challenge. *Nat. Chem.* **2016**, *8*, 202–204. (d) Zhang, Z.; Zhao, Z.; Hou, Y.; Wang, H.; Li, X.; He, G.; Zhang, M. Aqueous platinum(II)-cage-based light-harvesting system for photocatalytic cross-coupling hydrogen evolution reaction. *Angew. Chem., Int. Ed.* **2019**, *58*, 8862–8866.
- (2) (a) Wang, Q.-Q.; Gonell, S.; Leenders, S. H. A. M.; Dürr, M.; Ivanović-Burmazović, I.; Reek, J. N. H. Self-assembled nanospheres with multiple endohedral binding sites pre-organize catalysts and substrates for highly efficient reactions. *Nat. Chem.* **2016**, *8*, 225–230. (b) Bender, T. A.; Morimoto, M.; Bergman, R. G.; Raymond, K. N.; Toste, F. D. Supramolecular host-selective activation of iodoarenes by encapsulated organometallics. *J. Am. Chem. Soc.* **2019**, *141*, 1701–1706.
- (3) (a) Zhang, D.-W.; Ronson, T. K.; Nitschke, J. R. Functional capsules via subcomponent self-assembly. *Acc. Chem. Res.* **2018**, *51*, 2423–2436. (b) Ronson, T. K.; Meng, W.-J.; Nitschke, J. R. Design principles for the optimization of guest binding in aromatic-paneled $Fe^{II}_4L_6$ cages. *J. Am. Chem. Soc.* **2017**, *139*, 9698–9707.
- (4) (a) Cook, T. R.; Stang, P. J. Recent developments in the preparation and chemistry of metallacycles and metallacages via coordination. *Chem. Rev.* **2015**, *115*, 7001–7045. (b) Wiester, M. J.; Ulmann, P. A.; Mirkin, C. A. Enzyme mimics based upon supramolecular coordination chemistry. *Angew. Chem., Int. Ed.* **2011**, *50*, 114–137.
- (5) (a) Leenders, S. H. A. M.; Gramage-Doria, R.; de Bruin, B.; Reek, J. N. H. Transition metal catalysis in confined spaces. *Chem. Soc. Rev.* **2015**, *44*, 433–448. (b) Zhao, L.; Jing, X.; Li, X.-Z.; Guo, X.-Y.; Zeng, L.; He, C.; Duan, C.-Y. Catalytic properties of chemical transformation within the confined pockets of Werner-type capsules. *Coord. Chem. Rev.* **2019**, *378*, 151–187.
- (6) (a) Ortiz de Montellano, P. R. Hydrocarbon hydroxylation by cytochrome P450 enzymes. *Chem. Rev.* **2010**, *110*, 932–948. (b) Denisov, I. G.; Makris, T. M.; Sligar, S. G.; Schlichting, I. Structure and chemistry of cytochrome P450. *Chem. Rev.* **2005**, *105*, 2253–2277.
- (7) (a) Iyanagi, T.; Xia, C.-W.; Kim, J. J. P. NADPH–cytochrome P450 oxidoreductase: prototypic member of the diflavin reductase family. *Arch. Biochem. Biophys.* **2012**, *528*, 72–89. (b) Murataliev, M. B.; Feyereisen, R.; Walker, F. A. Electron transfer by diflavin reductases. *Biochim. Biophys. Acta, Proteins Proteomics* **2004**, *1698*, 1–26. (c) Feiters, M. C.; Rowan, A. E.; Nolte, R. J. M. From simple to supramolecular cytochrome P450 mimics. *Chem. Soc. Rev.* **2000**, *29*, 375–384.
- (8) (a) Vermilion, J. L.; Coon, M. J. Identification of the high and low potential flavins of liver microsomal NADPH–cytochrome P450 reductase. *J. Biol. Chem.* **1978**, *253*, 8812–8819. (b) Gutierrez, v.; Grunau, A.; Paine, M.; Munro, A.; Wolf, C.; Roberts, G.; Scrutton, N. Electron transfer in human cytochrome P450 reductase. *Biochem. Soc. Trans.* **2003**, *31*, 497–501.
- (9) Barnaba, C.; Taylor, E.; Brozik, J. A. Dissociation constants of cytochrome P450 2C9/cytochrome P450 reductase complexes in a lipid bilayer membrane depend on NADPH: a single-protein tracking study. *J. Am. Chem. Soc.* **2017**, *139*, 17923–17934.
- (10) Dubey, K. D.; Shaik, S. Choreography of the reductase and P450_{BM3} domains toward electron transfer is instigated by the substrate. *J. Am. Chem. Soc.* **2018**, *140*, 683–690.
- (11) Iyanagi, T. Molecular mechanism of metabolic NAD(P)H-dependent electron-transfer systems: the role of redox cofactors. *Biochim. Biophys. Acta, Bioenerg.* **2019**, *1860*, 233–258.
- (12) (a) Reichenbach-Klinke, R.; Kruppa, M.; König, B. NADH model systems functionalized with Zn(II)-Cyclen as flavin binding site-structure dependence of the redox reaction within reversible

aggregates. *J. Am. Chem. Soc.* **2002**, *124*, 12999–13007. (b) Cibulka, R.; Vasold, R.; König, B. Catalytic photooxidation of 4-methoxybenzyl alcohol with a flavin–zinc(II)–cyclen complex. *Chem. - Eur. J.* **2004**, *10*, 6223–6231.

(13) Roux, Y.; Ricoux, R.; Avenier, F.; Mahy, J.-P. Bio-inspired electron-delivering system for reductive activation of dioxygen at metal centres towards artificial flavoenzymes. *Nat. Commun.* **2015**, *6*, 8509.

(14) Cheaib, K.; Roux, Y.; Herrero, C.; Trehoux, A.; Avenier, F.; Mahy, J.-P. Reduction of a tris(picoyl)amine copper(II) complex by a polymeric flavo-reductase model in water. *Dalton Trans* **2016**, *45*, 18098–18101.

(15) (a) Zhao, L.; Wei, J.-W.; Lu, J.-H.; He, C.; Duan, C.-Y. Renewable molecular flasks with NADH models: combination of light-driven proton reduction and biomimetic hydrogenation of benzoxazinones. *Angew. Chem., Int. Ed.* **2017**, *56*, 8692–8696.

(b) Zhao, L.; Wei, J.-W.; Zhang, J.; He, C.; Duan, C.-Y. Encapsulation of a quinhydrone cofactor in the inner pocket of cobalt triangular prisms: combined light-driven reduction of protons and hydrogenation of nitrobenzene. *Angew. Chem., Int. Ed.* **2017**, *56*, 15284–15288.

(16) (a) Meunier, B.; de Visser, S. P.; Shaik, S. Mechanism of oxidation reactions catalyzed by cytochrome P450 enzymes. *Chem. Rev.* **2004**, *104*, 3947–3980. (b) Gallagher, A. T.; Lee, J. Y.; Kathiresan, V.; Anderson, J. S.; Hoffman, B. M.; Harris, T. D. A structurally-characterized peroxomanganese(IV) porphyrin from reversible O₂ binding within a metal–organic framework. *Chem. Sci.* **2018**, *9*, 1596–1603. (c) Kang, B.; Kurutz, J. W.; Youm, K. T.; Totten, R. K.; Hupp, J. T.; Nguyen, S. B. T. Catalytically active supramolecular porphyrin boxes: acceleration of the methanolysis of phosphate triesters via a combination of increased local nucleophilicity and reactant encapsulation. *Chem. Sci.* **2012**, *3*, 1938–1944.

(d) Oldacre, A. N.; Friedman, A. E.; Cook, T. R. A self-assembled cofacial cobalt porphyrin prism for oxygen reduction catalysis. *J. Am. Chem. Soc.* **2017**, *139*, 1424–1427. (e) Oldacre, A. N.; Crawley, M. R.; Friedman, A. E.; Cook, T. R. Tuning the activity of heterogeneous cofacial cobalt porphyrins for oxygen reduction electrocatalysis through self-assembly. *Chem. - Eur. J.* **2018**, *24*, 10984–10987. Oliveri, C. G.; Gianneschi, N. C.; Nguyen, S. T.; Mirkin, C. A.; Stern, C. L.; Wawrzak, Z.; Pink, M. Supramolecular allosteric cofacial porphyrin complexes. *J. Am. Chem. Soc.* **2006**, *128*, 16286–16296.

(17) Meng, W.-J.; Breiner, B.; Rissanen, K.; Thoburn, J. D.; Clegg, J. K.; Nitschke, J. R. A self-assembled M₈L₆ cubic cage that selectively encapsulates large aromatic guests. *Angew. Chem., Int. Ed.* **2011**, *50*, 3479–3483.

(18) Wang, C.-H.; Gao, W.-Y.; Powers, D. C. Measuring and modulating substrate confinement during nitrogen atom transfer in a Ru₂-based metal-organic framework. *J. Am. Chem. Soc.* **2019**, *141*, 19203–19207.

(19) (a) Page, C. C.; Moser, C. C.; Chen, X.-X.; Dutton, P. L. Natural engineering principles of electron tunnelling in biological oxidation–reduction. *Nature* **1999**, *402*, 47–52. (b) Yuasa, J.; Yamada, S.; Fukuzumi, S. A mechanistic dichotomy in scandium ion-promoted hydride transfer of an NADH analogue: delicate balance between one-step hydride-transfer and electron-transfer pathways. *J. Am. Chem. Soc.* **2006**, *128*, 14938–14948.

(20) Harriman, A.; Porter, G. Photochemistry of Manganese Porphyrins. *J. Chem. Soc., Faraday Trans. 2* **1979**, *75*, 1532–1542.

(21) Saleh, F. S.; Rahman, M. R.; Okajima, T.; Mao, L.; Ohsaka, T. Determination of formal potential of NADH/NAD⁺ redox couple and catalytic oxidation of NADH using poly(phenosafranin)-modified carbon electrodes. *Bioelectrochemistry* **2011**, *80*, 121–127.

(22) Johnson, J. A.; Petersen, B. M.; Kormos, A.; Echeverría, E.; Chen, Y.-S.; Zhang, J. A new approach to non-coordinating anions: Lewis acid enhancement of porphyrin metal centers in a zwitterionic metal–organic framework. *J. Am. Chem. Soc.* **2016**, *138*, 10293–10298.